Chinese Journal of
POLYMER SCIENCE

RESEARCH ARTICLE

https://doi.org/10.1007/s10118-026-3723-5
Chinese J. Polym. Sci.

Investigation of Bio-based Acrylate Reactive Diluents for UV-curable Electronic Packaging Polyurethane Adhesives

Yun-Tao Li[a,c], Shun-Peng Sun[c], Ya-Meng Jia[c], Shu-Sheng Li[a,b,c*], Chuan-Yong Zong[a,c], Xu-Bao Jiang[a], and Xiao-Li Zhu[a*]

[a] *College of Chemistry and Chemical Engineering, University of Jinan, Jinan 250022, China*
[b] *National Engineering Research Center for Colloidal Materials & Key Laboratory of Special Functional Aggregated Materials of Ministry of Education, School of Chemistry and Chemical Engineering, Shandong University, Jinan 250100, China*
[c] *Institute for UJN-SD Link New Material Research, Shandong Link Adhesive Co., Ltd., Jinan 251400, China*

Electronic Supplementary Information

Abstract Traditional acrylate reactive diluents, which are derived from fossil resources, are known to exhibit significant irritation and allergenic potential, leading to their prohibition in high-end electronics, particularly in wearable devices. To address these limitations, four bio-based acrylate reactive diluents (BRDs) were synthesized *via* the reaction of alcohols derived from renewable sources, piperitol, vanillin, eugenol, and isosorbide, with methacrylic anhydride. The viscosity of the synthesized BRDs and the T_g of their corresponding polymers were systematically evaluated and compared with those of the petroleum-based diluent isobornyl acrylate (IBOA). The BRDs were then blended with acrylate-terminated polyurethane (APU) to formulate a series of UV-curable polyurethane adhesives (APU-BRDs). The results suggest that BRDs effectively reduce the viscosity of APU. By selecting and combining BRDs, the bonding strength of APU-BRDs to polar substrates such as PC and glass can reach 20 MPa. Even for non-polar substrates like PE, the strength is close to 5 MPa. The values obtained in this study exceed those of adhesives prepared using the conventional petroleum-based diluent IBOA. Furthermore, the study explored the potential application of APU-BRDs in smart wearable devices, confirming their suitability for next-generation wearable technology.

Keywords Bio-based acrylate; Reactive diluents; Polyurethane; UV-curable adhesives; Electronic watch packaging

Citation: Li, Y. T.; Sun, S. P.; Jia, Y. M.; Li, S. S.; Zong, C. Y.; Jiang, X. B.; Zhu, X. L. Investigation of bio-based acrylate reactive diluents for UV-curable electronic packaging polyurethane adhesives. *Chinese J. Polym. Sci*. https://doi.org/10.1007/s10118-026-3723-5

INTRODUCTION

UV-curable polyurethane (UV-PU) adhesives represent a groundbreaking advancement, combining the exceptional properties of polyurethane adhesives, such as strong adhesion, wear resistance, and chemical corrosion resilience, with the efficiency and sustainability of UV-curing technology.[1,2] This integration enables rapid curing, energy efficiency, and environmental benefits, making UV-PU adhesives highly desirable in automotive, aerospace, and electronics industries.[3,4] However, the high viscosity of acrylate-terminated polyurethane oligomers (APU), the primary resin in UV-PU adhesives, often complicates their application. To address this, reactive diluents are incorporated to reduce the viscosity, improve the substrate wettability, and enhance the adhesion properties through active participation in the photocuring reaction.[5]

Traditional petroleum-based reactive diluents, such as IBOA, are limited by their potential to cause skin irritation and allergic reactions,[6,7] particularly in applications involving close human contact, such as wearable devices. In response, companies such as Apple have established strict guidelines prohibiting and restricting the use of such substances in smart wearable devices, prioritizing user safety and comfort. This has spurred interest in bio-based reactive diluents (BRDs) derived from renewable resources such as plant oils and natural aromatic compounds. BRDs offer environmental and health advantages, including reduced fossil-fuel dependence, lower emissions, biodegradability, and minimal toxicity.[8–11] Studies by researchers have demonstrated the potential of BRDs to replace traditional diluents while maintaining or enhancing performance. Wu *et al*.[12] synthesized a series of furan-based diacrylates, which significantly increased the T_g, hardness, and elastic modulus of cured coatings while maintaining low viscosity and good processability. In addition, the coatings exhibit excellent solvent resistance and high thermal stability. Dai *et al*.[13] synthesized 4-vinylguaiacol acetyl ester from ferulic acid. This compound combines the high copolymerization activity of the vinyl group, rigid structure of the aromatic ring, and low volatility. It not only significantly

* Corresponding authors, E-mail: chm_liss@ujn.edu.cn (S.S.L.)
E-mail: chm_zhuxl@ujn.edu.cn (X.L.Z.)
Received February 2, 2026; Accepted April 20, 2026; Published online July 22, 2026

improved the compatibility and processing flowability of the prepolymer, but also effectively enhanced the mechanical properties and thermal stability of the cured resin. Despite these advancements, developing BRDs that simultaneously exhibit excellent dilution ability and strong adhesive properties remains a significant challenge.

Resins (APU) constitute the fundamental component of adhesive systems and serve as the primary matrix for cross-linked network formation and performance enhancement. Through resin incorporation, adhesives can achieve superior mechanical strength, toughness, and thermal resistance, enabling diverse bonding applications. PU synthesized *via* the reaction of diol and isocyanate monomers exhibits tunable physical properties *via* selective monomer pairing. Polyester diols impart high strength and adhesion to PU, but poor tensile strength.[14] Conversely, polyether diols provide enhanced toughness but suffer from significant strength reduction.[15] To balance these properties, poly(diethylene glycol) adipate (PDGA) was chosen as the diol component. Its molecular architecture combines the strength-conferring ester groups with flexibility-enhancing ether linkages. Hexamethylene diisocyanate (HMDI) was selected owing to its non-yellowing characteristics during aging[16] and superior strength imparted by its bicyclic aliphatic structure compared to monocyclic alternatives such as isophorone diisocyanate.[17]

In this study, four novel BRDs, namely piperonyl methacrylate (PPA), vanillin methacrylate (VAA), eugenol methacrylate (EGA), and isosorbide methacrylate (ISA), were designed and synthesized as photocurable reactive diluents (Scheme 1a). Their structures and photo-polymerization kinetics were investigated thoroughly. APU was synthesized from PDGA and HMDI, and ended with hydroxyethyl acrylate (HEA) (Scheme 1b). The dilution efficiency of BRDs in APU was evaluated using rheological analysis. Subsequently, UV-PU adhesives were prepared by blending BRDs with APU and curing them under UV light (Scheme 1c), and their thermomechanical properties, mechanical performance, and basic adhesive properties were systematically characterized. This study aims to advance the development of sustainable high-performance UV-PU adhesives for smartwatch applications.

EXPERIMENTAL

Materials

Isobornyl acrylate (IBOA, 98%), piperitol (PP, 99%), vanillin (VA, 99%), eugenol (EG, 99%), isosorbide (IS, 99%), methacrylic anhydride (MAAn, 94%), dichloromethane (CH_2Cl_2, 99%), 3-glycidoxypropyltrimethoxysilane (KH560, 99%), and 4-dimethylaminopyridine (DMAP, 99%) were all purchased from Macklin Co., Ltd. Butylated hydroxytoluene (BHT, 99%), 2-hydroxy-2-methylpropiophenone (Irgacure 1173, 99%), dicyclohexylmethane diisocyanate (HMDI, 99%), benzoin dimethyl ether (BDK, 99%), 2,4,6-trimethyl-benzoyldiphenyl phosphine oxide (TPO, 99%), 2-hydroxy-ethyl acrylate (HEA, 99%), dibutyltin dilaurate (DBTDL, 99%), *N*,*N*-dimethylacrylamide (DMAA, 99%), trimethylol- propane triacrylate (TMPTA, 99%), and reolosil were all purchased from Aladdin Co., Ltd. Poly(diethylene glycol) adipate (PDGA, M_n=2000) was purchased from Covestro Co., Ltd.

Synthesis of BRDs and PolyBRDs

The BRDs were synthesized according to a previously reported method.[18,19] A typical reaction for the synthesis of VAA is as follows: VA of 0.10 mol (15.20 g) and DMAP of 2.4 mmol (0.29 g) were mixed in a flask, and bubbled with argon (Ar) for 1 h to remove H_2O and O_2 from the reaction system. Then, MAAn of 0.12 mol (18.48 g) was added and reacted at room temperature for 3 h and go on for 24 h at 45 °C. Subsequently, the mixture was

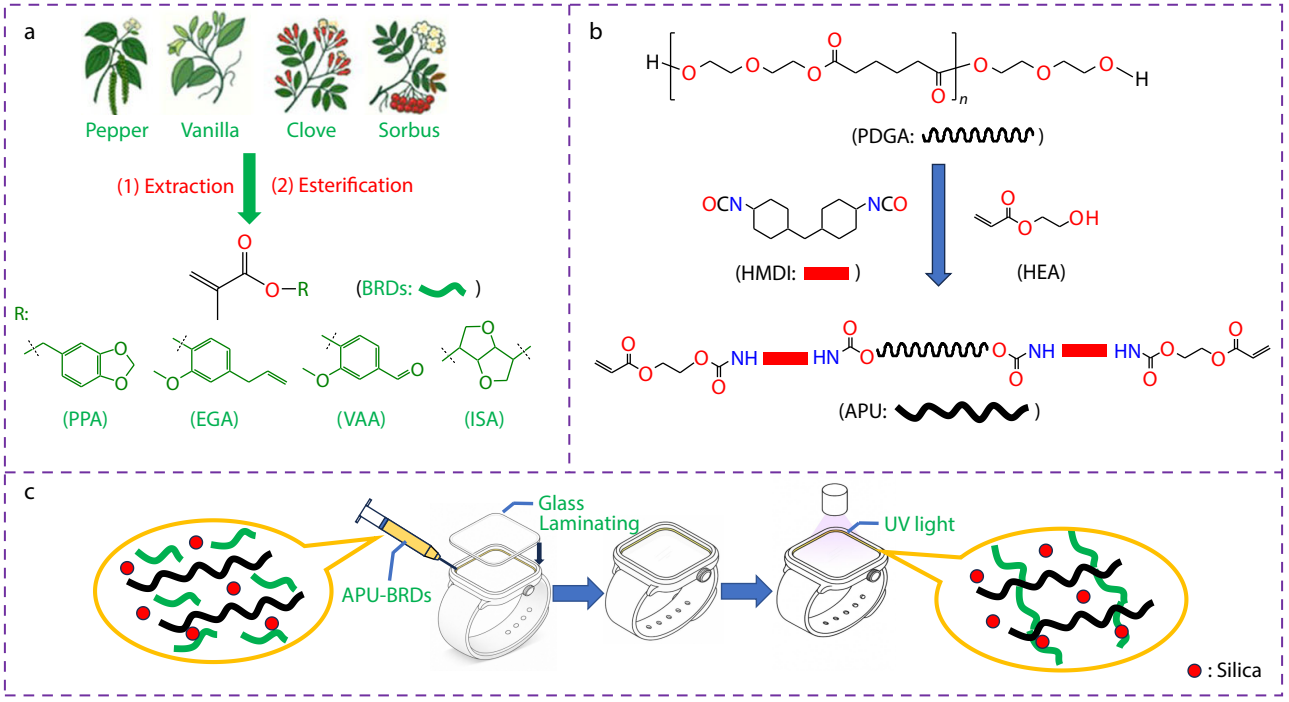

Scheme 1 Preparation process of (a) BRDs and (b) APU, and (c) schematic diagram of UV-PU adhesives.

https://doi.org/10.1007/s10118-026-3723-5

dissolved in 150 mL of CH_2Cl_2 and washed with 150 mL of saturated $NaHCO_3$ aqueous solution until no more carbon dioxide was produced to remove excess MAAn and methacrylic acid product. VAA with a yield of 85.2% was obtained after CH_2Cl_2 removed by vacuum distillation. PPA, EGA, and ISA were prepared from PP, EG, and IS using the same process, with yields of 89.4%, 86.6%, and 82.1%, respectively.

PPA: ^{1}H-NMR (400 MHz, $CDCl_3$, δ, TMS, ppm): 1.95 (t, J=1.2 Hz, 3H), 5.08 (s, 2H), 5.57 (dq, J=1.6 Hz, 1H), 5.95 (s, 2H), 6.14 – 6.11 (m, 1H), 6.88–6.74 (m, 3H); ^{13}C-NMR (δ, ppm): 167.25 (Cd), 147.79 (C4), 136.23 (Cb), 129.86 (C5), 125.58 (Ca), 121.59 (C2), 107.67 (C3), 101.16 (C6), 66.40 (C1), 18.71 (Cc).

EGA: ^{1}H-NMR (400 MHz, $CDCl_3$, δ, TMS, ppm): 6.98 (d, J=7.8 Hz, 1H), 6.81 (d, J=2.0 Hz, 1H), 6.79 (dd, J=7.8, 2.0 Hz, 1H), 6.42–6.31 (m, 1H), 5.98 (ddt, J=16.9, 10.1, 6.8 Hz, 1H), 5.78–5.71 (m, 1H), 5.18–5.05 (m, 2H), 3.82 (s, 3H), 3.40 (d, J=6.8 Hz, 2H), 2.13–2.03 (m, 3H); ^{13}C-NMR (δ, ppm): 165.63 (Cd), 151.01 (C6), 143.32 (C1), 138.91 (C4), 137.46 (C9), 135.65 (Cb), 127.13 (Ca), 123.19 (C3), 121.88 (C2), 116.13 (C10), 112.07 (C5), 56.30 (C7), 40.09 (C8), 18.21 (Cc).

VAA: ^{1}H-NMR (400 MHz, $CDCl_3$, δ, TMS, ppm): 9.96 (s, 1H), 7.51 (m, 1H), 7.48 (d, J=6.0 Hz, 1H), 7.26 (d, J=12.0 Hz, 1H), 6.39 (s, 1H), 5.81 (s, 1H), 3.89 (s, 3H), 2.08 (s, 3H); ^{13}C NMR (δ, ppm): 191.01 (C8), 164.74 (Cd), 152.04 (C1), 145.14 (C6), 135.10 (Cb), 128.43 (Ca), 124.29 (C3), 122.87 (C4), 111.19 (C2), 110.53 (C5), 56.51 (C7), 18.00 (Cc).

ISA: ^{1}H-NMR (400 MHz, $CDCl_3$, δ, TMS, ppm): 6.22– 6.16 (d, J=5.6 Hz, 1H), 6.13–6.10 (d, J=5.7 Hz, 1H), 5.73–5.59 (dd, J=12.7, 5.3 Hz, 2H), 5.29–5.16 (m, 2H), 4.55–4.52 (m, 1H), 4.05–3.87 (m, 4H), 2.02–1.94 (dd, J=20.3, 5.8 Hz, 6H); ^{13}C-NMR (δ, ppm): 163.09 (Cd), 135.68 (Cb), 129.31 (Ca), 86.25 (C3), 80.67 (C1), 73.32 (C2), 17.61 (Cc).

The cured polymers, polyBRDs (polyVAA, polyPPA, polyEGA, and polyISA), together with the contrast sample polyIBOA were obtained *via* UV-initiated BRDs radical polymerization using BDK/TPO (50/50 *W*/*W*) as the photo-initiator, under irradiation at 365 nm UV LED light source (Technigraf Amp) for 30 s, with an energy intensity of 500 mJ/cm^2.

Synthesis of APU

In a typical procedure, an APU oligomer is prepared *via* a two-step reaction. 80.0 g (40 mmol) of PDGA was added into the reactor. Trace water was then removed at 110 °C under vacuum for 2 h. After that, the temperature of the system was lowered to 90 °C, then 13.12 g (50 mmol) of HMDI and 0.06 g (0.10 mmol) of DBTDL was added. The reaction was allowed to proceed for 1 h at 90 °C. After that, 0.022 g (0.10 mmol) of BHT as the polymerization inhibitor and 2.32 g (20 mmol) of HEA was added as capping agent, and the reactor was then maintained at 80 °C for an additional 1 h of reaction to allow for complete capping. Finally, a viscous liquid, APU, was obtained.

Preparation of APU-BRDs Adhesives

APU-BRDs comprises APU (50.0 wt%), BRDs (22.5 wt%), DMAA (17.5 wt%), and other additives (10.0 wt%), such as thixotropic agent reolosil, silane coupling agent KH560 and photo-initiators BDK/TPO. The mixture was homogenized for 3 min using a high-speed disperser (2500 r/min) followed by three centrifugation cycles in a vacuum centrifuge (5 min each at 1500 r/min). The mixture was then irradiated for 30 s under a 365 nm UV-LED light source (Technigraf Amp) with an energy intensity of 500 mJ/cm^2. APU-BRDs adhesives were thus obtained and named APU-VAA, APU-PPA, APU-EGA, and APU-ISA. The APU-IBOA adhesive was obtained using the same method.

Characterization

FTIR and NMR

The chemical structures of BRDs and APU, along with their precursors, were characterized by Fourier transform infrared spectroscopy (FTIR, Tensor 27, Brüker, USA) and nuclear magnetic resonance (NMR, Advance III, 400 MHz, Brüker, USA). FTIR was performed in the range of 4000–400 cm^{-1} with a resolution of 4 cm^{-1}. The BRDs were dispensed onto KBr pellets, and the cured APU-BRDs were tested using the ATR mode. ^{1}H-NMR spectroscopy was performed in DMSO-d_6 or $CDCl_3$ at a concentration of 5 mg/mL.

Viscosity measurement

The viscosities of the BRDs, IBOA, TMPTA, DMAA, APU, APU-BRDs, and APU-IBOA were measured using a rheometer (Bohlin DV2T, Brookfield, USA) equipped with a CZ-52 disk. Measurements were conducted at a constant rotational speed of 1 r/min and 10 r/min, maintained at 25 °C for 2 min. The viscosity was determined in triplicate and the average value was reported. Additionally, viscosity data were collected as a function of the shear rate $\dot{\gamma}$ (s^{-1}) and analyzed using Eq. (1):

$$\eta(\dot{\gamma}) = \eta_\infty + (\eta_0 - \eta_\infty)\left[1 + (\lambda\dot{\gamma})^a\right]^{\frac{n-1}{a}} \quad (1)$$

where $\eta(\dot{\gamma})$ (mPa·s) is the apparent viscosity at shear rate $\dot{\gamma}$, η_0 (mPa·s) and η_∞ (mPa·s) represent the zero- and infinite-shear viscosities, respectively. λ (s) is the characteristic time constant, a is the Yasuda parameter describing the breadth of the transition region, and n is the flow behavior index.

Differential scanning calorimeter

The glass transition temperatures (T_g) of polyBRDs and cured APU-BRDs adhesives were measured using a differential scanning calorimeter (DSC, DSC25, TA Instruments, USA) under N_2 atmosphere at a heating rate of 10 °C/min.

Dynamic mechanical analysis

Dynamic mechanical analysis (DMA, DMA-Q800, TA Instruments, USA) of the cured APU-BRDs adhesives was conducted in single cantilever mode. The temperature range was 30–200 °C with a heating rate of 1 °C/min at frequency of 1 Hz and a displacement of 0.01 mm.

Thermogravimetric analysis

Thermogravimetric analysis (TGA, TGA55, TA Instruments, USA) of the cured APU-BRDs adhesives was performed under N_2 (35 mL/min). Approximately 10 mg of the sample was heated from 25 °C to 600 °C at a rate of 10 °C/min.

Shore hardness

The APU-BRDs were injected into a mold with a depth of 1 cm and a radius of 0.5 cm, and cured completely under UV light for 30 s. The cured polymer was removed and cooled to room temperature. The Shore hardness was measured using a Shore hardness tester (Shore D, Nscing Es, GER).

Mechanical properties

Stress-strain tests of the cured APU-BRDs were conducted at room temperature using a universal testing machine (KJ-1066A, Guangdong Kejian Instrument, China) with a fixed tensile rate of 300 mm/min.

Toughness

The tensile toughness of the samples can be defined by integrating the area under the engineering stress-strain curves, and measured at a stretching speed of 300 mm/min using Eq. (2):

$$\text{Toughness (MJ/m}^3\text{)} = \int_0^{\varepsilon_{max}} \sigma d\varepsilon \quad (2)$$

where σ is the engineering stress, ε is the engineering strain, ε_{max} is the elongation at the break of the sample.

Crosslink density

DMA was employed to determine the crosslink density (v_e, mol/m^3) of the cured APU-BRDs, according to Eq. (3):[20, 21]

$$v_e = \frac{E'}{3RT_0} \quad (3)$$

where E' (Pa) represents the storage modulus corresponding to the absolute temperature (T_0, K) of the rubbery plateau region, and R represents the gas constant (8.314 J/(mol·K)).

Gel content

The gel content of the cured APU-BRDs was determined using the following procedure. The dry samples (m_i) were immersed in toluene for 1 week and weighed (m_f) after thorough drying. The gel content (GC) was calculated using Eq. (4):

$$\text{GC (\%)} = \frac{m_f}{m_i} \times 100 \quad (4)$$

Conversion rate

The double bond conversion rates of photo-initiated PPA, EGA, VAA, and ISA radical polymerizations can be calculated by comparing the changes in the transmittance of the C=C double bonds.[22,23] Conversion rate (α) was calculated according to Eq. (5):

$$\alpha = 1 - \frac{\left(\frac{T_{(C=C)}}{T_{ref}}\right)_t}{\left(\frac{T_{(C=C)}}{T_{ref}}\right)_0} \quad (5)$$

where $T_{(C=C)_t}$ and $T_{(C=C)_0}$ are the transmittances of the C=C stretching vibration peak in the acrylic ester group at time t and the initial time, respectively; T_{ref_t} and T_{ref_0} are the transmittances of the calibration peak at time t and the initial time, respectively. The calibration peaks for PPA, VAA, and EGA corresponded to the stretching vibration peak of the aromatic ring at 1500 cm^{-1}. The calibration peak for ISA corresponds to the stretching vibration peak of the carbonyl group at 1720 cm^{-1}.

Direct peptide reactivity assay (DPRA)

DPRA was conducted according to the standard operating procedure mentioned in OECD TG 442C (details are provided in Fig. S1 and Table S1 in the electronic supplementary information, ESI).[24]

Curing shrinkage

A cylindrical mold (1 × 0.1 cm) was filled with APU-BRDs, and a scraper was used to level the surface, ensuring a consistent volume of uncured material. The sample was fully cured under identical UV-curing conditions. The curing shrinkage (%) before and after curing was calculated based on the density method using Eq. (6):

$$\text{Curing shrinkage (\%)} = \left(1 - \frac{m_a(m_a - m_l)}{V\rho_l m_a}\right) \times 100 \quad (6)$$

where m_a and m_l are the masses of the APU-BRDs in air and liquid, respectively, V is the volume of the module, and ρ_l is the density of the deionized water used in the test at 25 °C.

Lap shear test

The adhesive strength of the APU-BRDs was measured using a lap-shear adhesion test. The APU-BRDs were uniformly applied to the substrate surfaces (PC, glass, PMMA, PET, and PE) covering an area of 25 mm × 2 mm. The spacers were positioned along both sides of the bonding region to maintain a consistent adhesive thickness of 0.20 mm. A second substrate (glass) was carefully aligned over the adhesive-coated area to form a single-lap shear joint. Light pressure was applied to ensure a uniform adhesive distribution and eliminate visible air bubbles or voids. The assembled specimen was then irradiated for 30 s using a 365 nm UV light source directed at the overlap region to achieve complete curing. Both ends of the specimen were clamped into an electronic universal testing machine (KJ-1066A, Guangdong Kejian Instruments, China), and shear tests were conducted at a crosshead speed of 5 mm/min to determine the bond strength of the APU-BRDs on each substrate.

Solvent resistance assessment

The solvent resistance assessment was conducted according to the following method: single-lap shear joints were prepared using glass and PC substrates bonded with either APU-BRDs or APU-IBOA over a lap area of 25 mm × 2 mm. The joints were immersed in distilled water and glycerol at 25 °C for 7 days. After immersion, the specimens were retrieved and any residual solvent was removed from the surface. Shear performance was evaluated using the same method.

RESULTS AND DISCUSSION

Synthesis and Structure Characterization of BRDs

As shown in Fig. S2 (in ESI), BRDs, namely VAA, PPA, EGA, and ISA, were obtained by the DMAP-catalyzed esterification of MAAn with bio-alcohols/phenols, VA, PP, EG, and IS, respectively. DMAP is an effective nucleophilic base catalyst for the esterification of alcohols with acid anhydrides[25] and other related reactions. The resonance of the electron-donating dimethylamino group with the pyridine ring can strongly activate the ammonia atoms in the ring for nucleophilic substitution and significantly catalyze the esterification of alcohols and acids with high resistance and low reactivity. The currently accepted mechanism for the acylation reactions of alcohols involves the pre-equilibrium formation of an acyl-pyridinium cation through the reaction of DMAP with the acyl donor. The alcohol then reacts with the acylated catalyst in the rate-determining step to form the ester product together with the deactivated (protonated) catalyst.[25] PPA, EGA, and VAA are pale yellow liquids, which can be attributed to their benzene ring structures. In contrast, the ISA is a colorless, transparent liquid. Its aliphatic ring structure contributed to its strong resistance to yellowing (Fig. S3 in ESI).

The FTIR spectra of the BRDs with their precursors are shown in Fig. S4 (in ESI). In the MAAn spectrum, the peaks at 1786 cm^{-1} and 1726 cm^{-1} belong to the stretching vibration of C=O, and double bands are formed due to vibration coupling.[26] The band at 1636 cm^{-1} corresponds to the C=C stretching vibration. In the PP, EG, VA, and IS spectra, wide bands between 3100–3500 cm^{-1} are typical stretching vibra-

tion absorptions of —OH and 1100 cm^{-1} for C—O (alcohols).[9] Obviously, in the obtained BRDs (Fig. S4 in ESI), the —OH disappeared, and the C=O peak shifted to a lower wavenumber after esterification,[10,27] and the C=C stretching vibration absorption peak was observed at approximately 1636 cm^{-1}.[28]

The structures of the BRDs with their precursors MAAn, PP, EG, PA, and IS were analyzed using ^{1}H-NMR and ^{13}C-NMR (Fig. 1 and Fig. S5 in ESI). In ^{1}H-NMR spectrum of MAAn (Fig. S5 in ESI), and three peaks at 6.24 ppm (Ha), 5.83 ppm (Ha') and 2.01 ppm (Hc) belong to the methacrylate group.[10] In its ^{13}C-NMR spectrum, characteristic peaks of methacrylate group appear at 129.33 ppm (Ca), 135.69 ppm (Cb), 17.59 ppm (Cc) and 163.04 ppm (Cd).[26] In the NMR spectra of the BRDs (Fig. 1 and Fig. S5 in ESI), we can clearly observe the absorption peaks belonging to these biomass raw materials, as well as the characteristic peaks of the methacrylate group in MAAn. Additionally, when the hydroxyl groups of biomass alcohols form ester groups with MAAn, the H atoms of CH_2 in PPA and CH in ISA adjacent to the hydroxyl groups shift to lower positions owing to the electron-withdrawing effect. The NMR spectrum confirmed the successful synthesis of BRDs.

The main function of the BRDs is to reduce the viscosity of the system. Their apparent viscosities were measured at 25 °C and compared them with those of traditional reactive diluents, such as IBOA, TMPTA, and DMAA (Fig. 2a). As shown in Fig. 2(a), the viscosities of PPA, EGA, VAA, and ISA are 5.3, 30.4, 35.1 and 5.2 mPa·s. The viscosities of PPA and ISA were similar to that of IBOA (8.5 mPa·s) and smaller than that of DMAA (12.0 mPa·s). Although the viscosities of EGA and VAA were relatively higher than those of some dual-functional active diluents and significantly lower than those of the tri-functional TMPTA (108.0 mPa·s).

All the four BRDs contained methacrylate groups. Thus, this pronounced viscosity variation arises from structural differences in the bio-alcohol components. VAA possesses a high-dipole-moment aldehyde group (H—C=O), which increases the cohesive energy density. Furthermore, its aromatic ether linkage (C—O—C) provides additional dipole-dipole interactions, resulting in the highest viscosity. In contrast, substituting the aldehyde in EGA with a less polar allyl group lowered its viscosity. However, this reduction was modest, suggesting that the aromatic ether bond significantly contributed to the relatively high viscosities observed for both VAA and EGA. Conversely, PPA and ISA exhibit substantially lower viscosities, primarily because of their high molecular symmetry. In PPA, the oxygen atoms within the 1,3-dioxolane ring increase the *π*-electron density of the aromatic ring *via* electron donation. This enhanced electron density creates electrostatic repulsion that impedes optimal π-π stacking between parallel

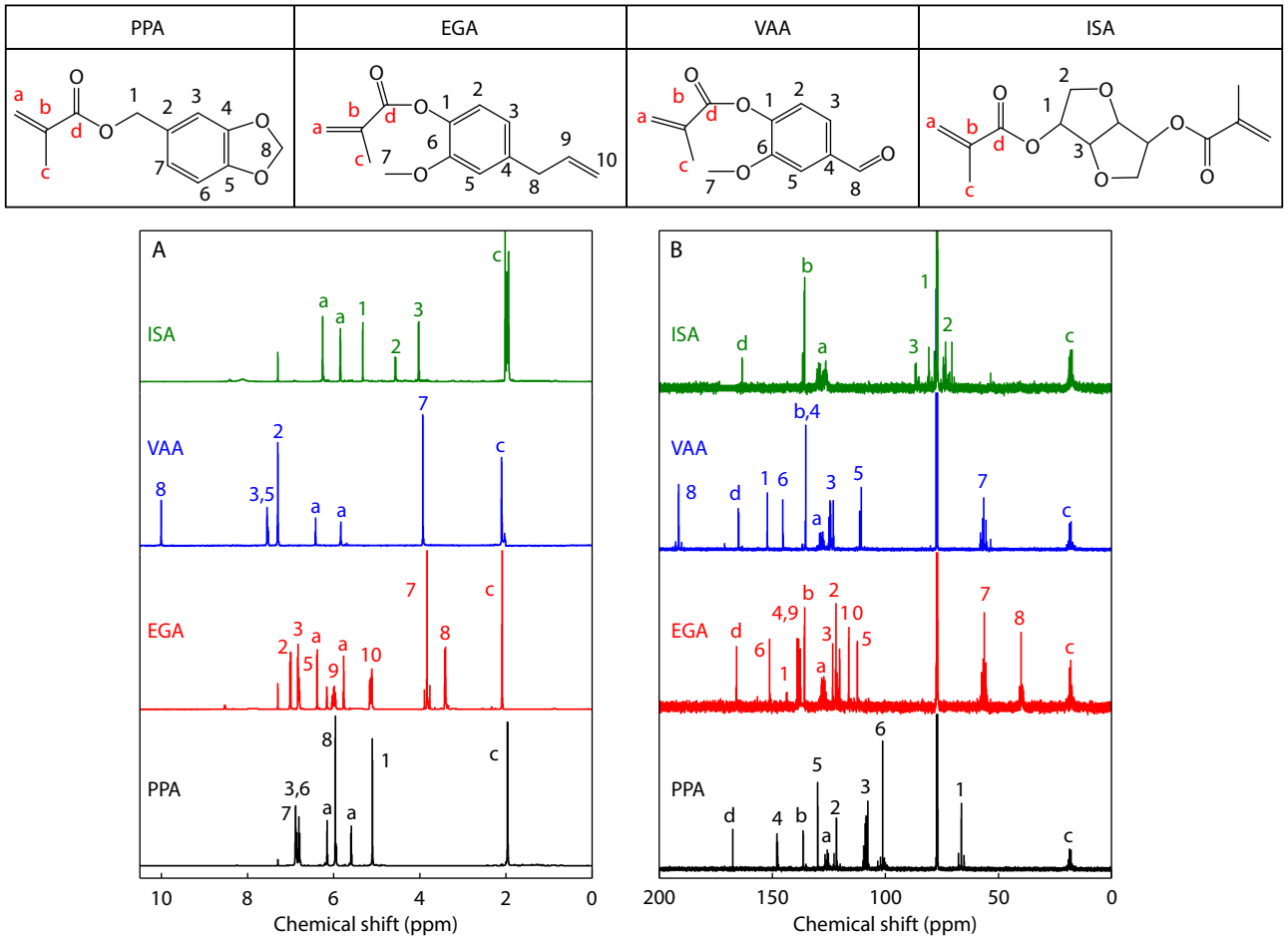

Fig. 1 (A) ^{1}H-NMR and (B) ^{13}C-NMR spectra of PPA, EGA, VAA, and ISA.

https://doi.org/10.1007/s10118-026-3723-5

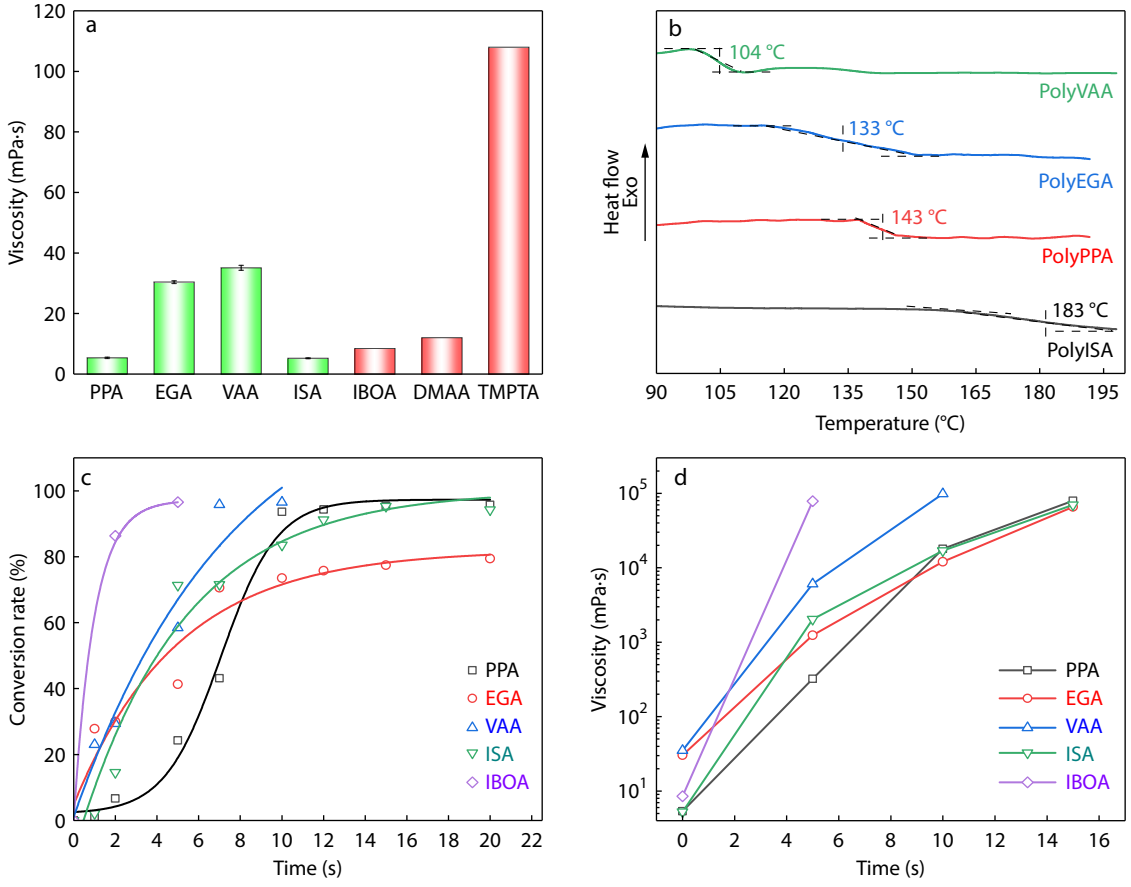

Fig. 2 (a) Viscosity of VAA, PPA, EGA and ISA compared with IBOA, DMAA, TMPTA; (b) DSC curves of polyVAA, polyPPA, polyEGA and polyISA; (c) Conversion rate-time curve and (d) viscosity changes for each BRDs and IBOA during UV curing.

aromatic rings, reducing intermolecular friction, and facilitating molecular sliding. The ISA displays even greater symmetry with the terminal ester groups. The rigidity of the isosorbide skeleton, combined with the spatial cancellation of the dipoles associated with the two carbonyl groups, results in an overall low dipole moment and weak intermolecular force.[29]

T_g of polyBRDs

The T_g is a key determinant of polymer performance in practical applications. The T_g values of polyBRDs were determined by DSC (Fig. 2b), and the values of polyVAA, polyEGA, polyPPA, and polyISA were 104, 133, 155, and 183 °C, respectively. These values are similar or higher than those of traditional diluent polymers such as polyIBOA (150 °C)[30] and polyDMAA (118 °C)[31] as reported in previous studies.

The T_g of polyBRDs correlates strongly with the pendant group architecture, increasing with increases in rigidity, steric bulk, polarity, and crosslinking potential. For instance, polyVAA (T_g, 104 °C) derives modest polarity from its —OCH_3 and —CHO substituents, which facilitate dipole-dipole interactions. The larger side groups provided steric hindrance, restricting the movement of the molecular chain to some extent. PolyEGA exhibits reduced polarity due to allyl substitution (compared to —CHO in polyVAA) but achieves higher T_g (133 °C) through radical-mediated crosslinking during polymerization, despite the lower reactivity of its allyl groups compared to acrylate. PolyPPA (T_g, 143 °C) benefits from a 1,3-dioxolane, which severely restricts chain rotation. The flexibility introduced by the benzyl ether linkage is insufficient to counteract this rigidity.[32,33] PolyISA demonstrated the highest T_g (183 °C) in the series, attributable to two synergistic factors: (1) its cyclic side-group architecture, which imposes steric constraints and enables directional hydrogen bonding, and (2) its bifunctional monomer, which fosters a densely crosslinked network.[34] These structure-property relationships provide a foundation for rationally designing polyBRDs with tailored T_g values and crosslink densities to meet specific application requirements.

UV reaction kinetics

The double bond conversion versus irradiation time for reactive diluents revealed a complex interplay between the monomer structure and polymerization kinetics. For BRDs and IBOA with BDK/TPO (5.0 wt%) under UV light (365 nm), FTIR monitored real-time changes in acrylate group absorption at 1636 cm^{-1}, enabling conversion rate calculations (Fig. S6 in ESI). As the duration of UV exposure increased, the intensity of the double-bond peak decreased (Fig. S6 in ESI), the conversion rates of the double bonds were calculated at different times (Fig. 2c).

Clearly, IBOA exhibits a faster curing rate, reaching nearly 100% conversion in just 2 s, which is significantly faster than BRDs. This difference arises because IBOA contains acrylate groups, whereas the BRDs are based on methacrylate groups. The steric hindrance in BRDs slows down the curing process

compared to IBOA. In BRDs, the polymerization rate of VAA was the highest (about 100% in 9 s). Its aldehyde group makes the double bond very reactive (electron-withdrawing)[35,36] and causes the solution to thicken quickly, leading to strong auto-acceleration. ISA showed similar kinetics to VAA, but much slower (about 100% in 20 s). Its rigid structure creates steric hindrance and slows the chain growth.[28] However, its ring rigidity and crosslinking later promoted viscosity build-up and auto-acceleration. EGA performed worst (<100%) even after 20 s. The allylic C—H bonds are readily abstracted by the propagating radicals, generating stable allylic radicals that cause chain termination.[37] Its flexible side chain also keeps the viscosity low for longer, preventing early auto-acceleration and making polymerization gradual. PPA has unique two-stage kinetics: a slow start (about 5 s induction) and rapid acceleration. The 1,3-dioxolane group initially "scavenges" radicals, but then creates crosslinks or new radicals, suddenly boosting the reaction rate and viscosity (enhancing auto-acceleration).[38] The change in viscosity during UV irradiation was consistent with the change in conversion rate (Fig. 2d).

Synthesis and Characterization of APU

The APU was synthesized in two steps (Fig. S7 in ESI). First, PDGA and HMDI reacted with each other through the hydroxyl and isocyanate groups using DBTDL as a catalyst to form —NCO terminated prepolymers. Then, the prepolymers reacted with HEA to obtain APU with acrylate group terminations, and BHT was used to avoid the self-polymerization of double bonds.

Structural characterization of APU, as well as its precursor PDGA and the prepolymer synthesized from PDGA with excess HMDI, was performed using FTIR (Fig. S8 in ESI). The PDGA spectrum displayed characteristic absorptions at 2933 and 2871 cm^{-1} (methylene antisymmetric/symmetric stretching), 1733 cm^{-1} (ester C=O stretching), and 1134 cm^{-1} (ether C—O—C stretching). The polymer exhibited —N=C=O stretching at 2270 cm^{-1}, N—H bending at 1540 cm^{-1} and urethane N—H stretching at 3370 cm^{-1}. Subsequent end-capping with HEA introduced UV-curable acrylate functionality, as evidenced by the disappearance of the 2270 cm^{-1} peak and emergence of C=C stretching at 1632 cm^{-1}.[14,15,39]

The ^{1}H- and ^{13}C-NMR spectra of APU and its precursors (PDGA, HMDI, and HEA) are presented in Fig. 3. In the ^{1}H-NMR spectrum of PDGA, four signals of equal integrated intensities were observed at 4.22, 3.66, 2.35, and 1.52 ppm. These are assigned, from low to high field, to proton H2 adjacent to the ester group in the diethylene glycol segment, H1 next to the ether group,[40] H4 bonded to the carbonyl group in adipic acid, and H5 at the neighboring methylene unit.[41] This trend reflects the relative electron-withdrawing strengths of esters > ethers > carbonyls. In HMDI, the —NCO group exerts both an electron-withdrawing effect and magnetic anisotropy, shifting the adjacent Hb proton downfield to 3.24 ppm. In contrast, the methylene protons Hf appear at 0.91 ppm due to the electron-donating influence of the two aliphatic six-membered rings. The signals between 1.01 and 2.10 ppm are attributed to the ring protons Hc–He.[42] For HEA, the characteristic vinyl protons of the *α,β*-unsaturated carbonyl compounds are clearly visible at 6.31 ppm (H*α*), 6.06 ppm (H*β*), and 5.79 ppm (H*α*').[43–45] The methylene protons adjacent to the ester and hydroxyl groups in HEA give rise to signals at 4.17 ppm (H*δ*) and 3.74 ppm (He), respectively.[46] In the spectrum of APU, all key features are present: the characteristic signals from PDGA (H1–H5), absorption peaks corresponding to the aliphatic rings of HMDI (Hb–Hf), and vinyl protons from HEA (H*α*, H*α*', H*β*).

The ^{13}C-NMR results were consistent with those of the ^{1}H-NMR analysis. The PDGA spectrum displayed five characteristic signals. The carbonyl carbon (C3) appears at 173.14 ppm. In descending order of chemical shift other signals are 68.62 ppm (C2), 63.42 ppm (C1),[40] which is adjacent to the ester group and ether group in the diethylene glycol segment, 33.17 ppm (C4) and 23.64 ppm (C5), bonded to the carbonyl

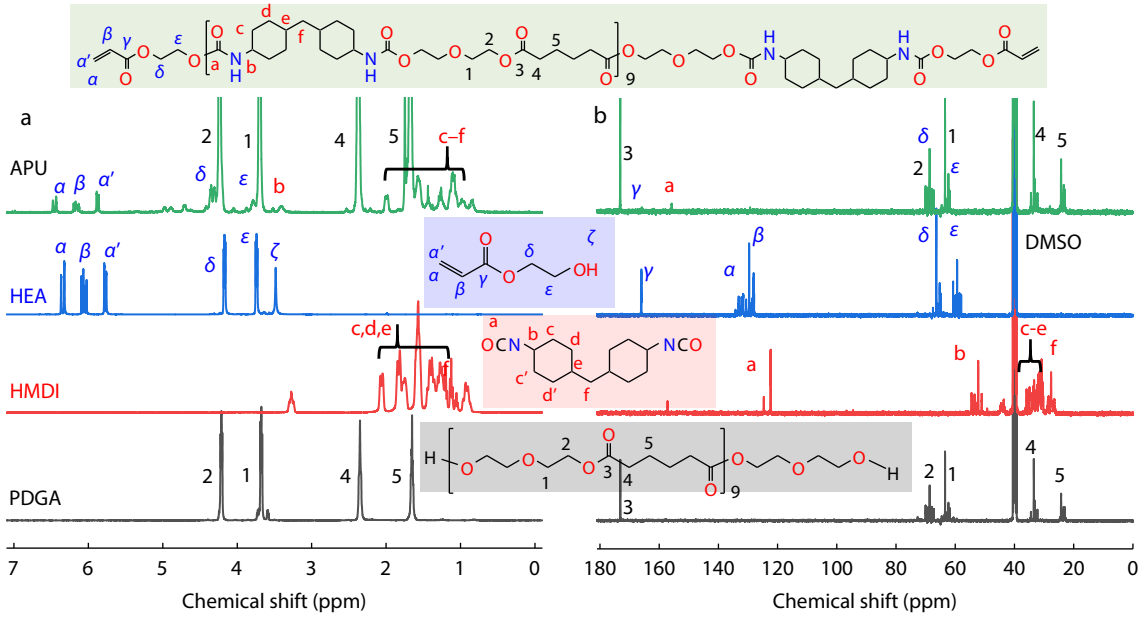

Fig. 3 (a) ^{1}H-NMR and (b) ^{13}C-NMR spectra of APU with its raw materials PDGA, HMDI and HEA.

https://doi.org/10.1007/s10118-026-3723-5

group in adipic acid. For HMDI, characteristic resonances are observed at 123.14 ppm (Ca in —NCO), 52.78 ppm (Cb attached to —NCO), and 27.63 ppm (methylene Cf), while signals in the range of 34.37–30.54 ppm correspond to carbon Cc–Ce of the cyclohexyl ring.[42] In the spectrum of HEA, the unsaturated alkene carbons C*α* and C*β* appear at 132.75 ppm and 128.64 ppm, respectively, the carbonyl carbon C*γ* is observed at 166.06 ppm, and the methylene carbons C*δ* and C*ε* give rise to signals at 66.01 and 59.33 ppm.[45] Importantly, in the spectrum of the final APU product, all characteristic signals from PDGA and most of those from HEA were clearly present. Moreover, the —NCO carbon (Ca) in HMDI from 123.14 ppm shifts downfield to 155.95 ppm in —NHCOO— carbon (Ca).[42] Together, these spectral data confirm the successful synthesis of APU.

Curing of APU-BRDs

The viscosity variations of the APU (containing other additives) before and after the incorporation of BRDs or IBOA (22.5 wt%) were measured at 25 °C, and their corresponding thixotropic indices (Ti) were calculated (Fig. 4a and Table S2 in ESI). In the absence of any BRDs, APU exhibited a very high viscosity, measuring 3.57×10^5 mPa·s at 1 r/min and 0.71×10^5 mPa·s at 10 r/min, with a Ti of 5.0. Upon addition of BRDs or IBOA, the resulting systems, APU-PPA, APU-EGA, APU-VAA, APU-ISA, and APU-IBOA, showed a significant reduction in viscosity. At 1 r/min, the viscosities decreased to 5.24×10^4 mPa·s, 9.85×10^4 mPa·s, 7.62×10^4 mPa·s, 7.7×10^4 mPa·s, and 5.72×10^4 mPa·s, respectively, corresponding to reduction rates of 85.3%, 72.4%, 78.7%, 78.4%, and 84.0%. At 10 r/min, the viscosities further decreased to 1.22×10^4 mPa·s, 1.99×10^4 mPa·s, 1.60×10^4 mPa·s, 1.64×10^4 mPa·s, and 1.21×10^4 mPa·s. These results indicate that BRDs possess excellent dilution efficacy comparable to that of IBOA. Furthermore, owing to the incorporation of fumed silica in the APU-BRDs systems, the formulations demonstrated pronounced thixotropic behavior, with Ti values exceeding 4. This property imparts a shear-thinning characteristic to the adhesive, enabling it to maintain a high viscosity at rest to prevent sagging while reducing viscosity under shear for ease of application.[47]

We also monitored the viscosity changes of the APU-BRDs and APU-IBOA (without initiators) at different temperatures. As expected, with increasing temperature, enhanced molecular thermal motion and reduced intermolecular forces led to a gradual decrease in viscosity (Fig. S9 in ESI). Furthermore, the viscosities of the APU-BRDs were recorded at different shear rates (Fig. S10 in ESI) and analyzed using the Carreau-Yasuda model (Eq. 1, Table S3 in ESI). The results show that their variation trends are similar: the viscosity decreases sharply as the shear rate increases, particularly within the range of 0.1 to 100 s^{-1}. All formulations exhibited shear-thinning behavior (n<1), with the EGA and ISA formulations exhibiting slightly

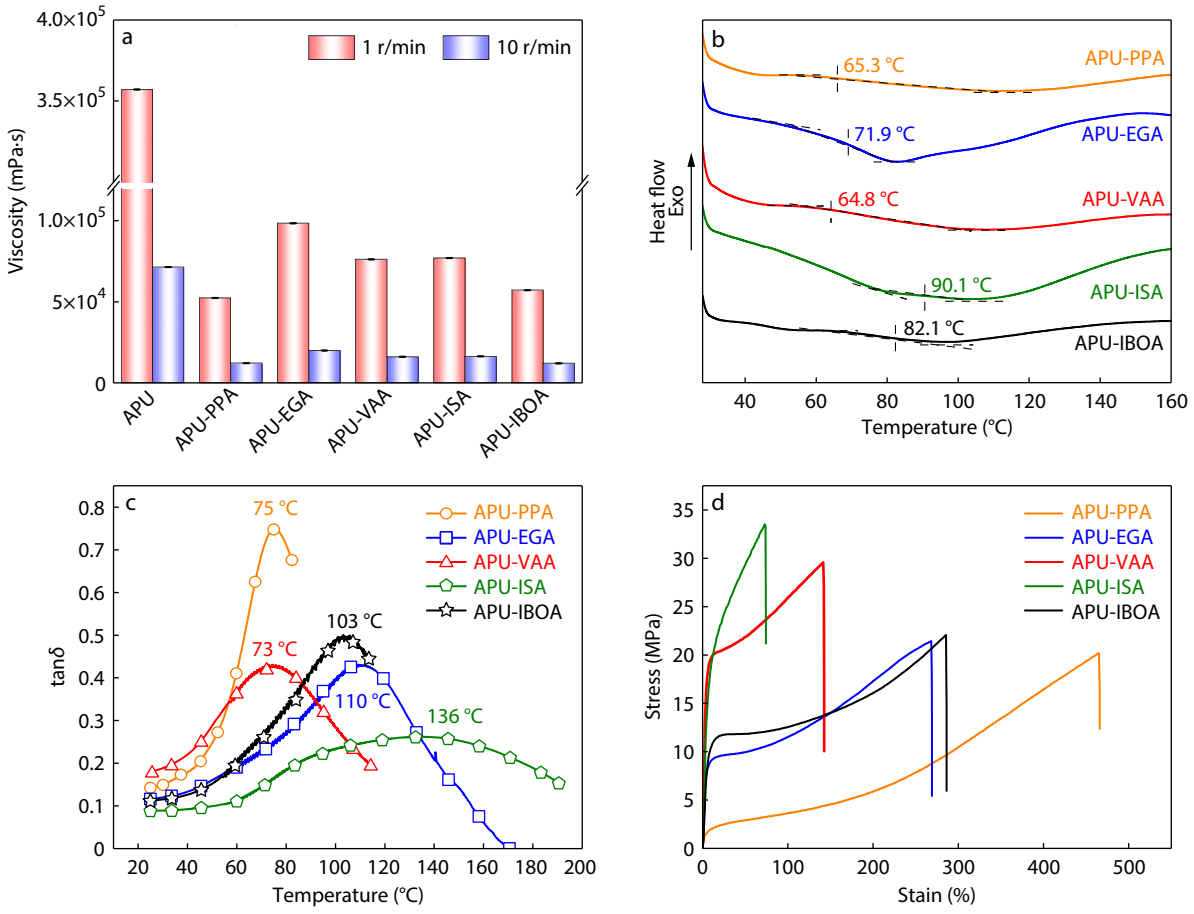

Fig. 4 (a) Viscosity of APU, APU-BRDs, and APU-IBOA, (b) DSC curves, (c) tan*δ*, and (d) stress-strain curves of APU-BRDs, and their comparation with APU-IBOA.

https://doi.org/10.1007/s10118-026-3723-5

stronger shear-thinning characteristics.

The T_g values of the UV-cured APU-BRDs and APU-IBOA were determined using DSC (Fig. 4b) and DMA (Fig. 4c), and the results are listed in Table S4 (in ESI). According to the DSC results, APU-IBOA exhibited a T_g of 82.1 °C. Among the APU-BRDs, APU-ISA demonstrated the highest T_g at 90.1 °C, followed by APU-EGA at 71.9 °C, while APU-PPA and APU-VAA showed comparable values of 65.3 °C and 64.8 °C, respectively. The elevated T_g of APU-ISA can be attributed to its rigid bicyclic tetrahydrofuran structure of ISA, which imparts significant steric hindrance and stiffness owing to its bridged cyclic ether linkages. Furthermore, as a bifunctional monomer, ISA enhances the crosslinking density of the system, thereby increasing the T_g. In contrast, EGA contains one acrylate group and one allyl group. The allyl group participates in photopolymerization, leading to additional crosslinking.[37] The DMA curves provided a clearer indication of the T_g values, which were generally higher than those obtained by DSC; however, the overall trends remained consistent.

The mechanical properties of the APU-BRDs and APU-IBOA were evaluated (three times for each sample) and compared (Fig. 4d, Table S5 in ESI). APU-IBOA displayed a tensile strength of (22.0±0.9) MPa and an elongation at break of 285%±14%. Among the APU-BRDs, APU-ISA demonstrated the highest tensile strength of (33.4±1.1) MPa but the lowest elongation at break of 82%±6%, resulting in the lowest toughness of (18.6±0.4) MJ/m^3. This strong yet brittle behavior is likely due to its high crosslinking density and rigidity. In comparison, APU-VAA exhibited a slightly lower tensile strength of (29.5±1.0) MPa, with an elongation at break of 145±9% and toughness of (33.2±0.3) MJ/m^3. APU-EGA showed properties similar to APU-IBOA, with a tensile strength of (21.2±0.7) MPa, elongation at break of 275%±12%, and toughness of (37.1±0.3) MJ/m^3, indicating a strong and tough mechanical performance. Following elastic deformation, both APU-EGA and APU-IBOA exhibit distinct yield points and broad cold-drawing regions, which are characteristic of forced elastic deformation. APU-PPA presented soft and tough characteristics, with a tensile strength of (20.1±0.8) MPa, the highest elongation at break of 470%±18%, and toughness of (40.9±0.5) MJ/m^3. The varied mechanical properties of the APU-BRDs provide a range of options for tailoring materials to meet specific application requirements. Table S5 (in ESI) shows that the Shore hardness of APU-PPA was 45±1, whereas that of other APU-BRDs was approximately 60. Except for the relatively low curing depth of APU-VAA (3.9±0.7 mm), the curing depths of other APU-BRDs are all close to 5 mm, which can all meet the requirements of curing depth for smartwatches.

Curing shrinkage is critical for adhesive performance, particularly for precision electronic devices. We measured the curing shrinkage of the APU-BRDs and compared it with that of APU-IBOA. As shown in Fig. S11 (in ESI), APU-PPA exhibited a curing shrinkage of 2.46%±0.10%, which was lower than that of APU-IBOA (3.65%±0.21%). The curing shrinkage values for APU-EGA, APU-VAA, and APU-ISA are 5.89%±0.05%, 4.70%±0.10%, and 6.84%±0.11%, respectively. The higher shrinkage observed for APU-ISA is attributed to its bifunctional groups. The curing shrinkage ranges obtained in this study are generally comparable to those reported in the literature for petroleum-based acrylic systems and acrylate-terminated polyurethanes, which typically fall between 2% and 10%.[48,49]

The crosslinking density (ν_e) of the polymer networks was determined using the DMA method, according to Eq. (3). The DMA curves of APU-BRDs and APU-IBOA are shown in Fig. S12 (in ESI) and the calculated ν_e values are listed in Table S4 (in ESI). An increase in ν_e restricts the chain mobility, thereby reducing the deformability of the material under stress and enhancing the modulus, as supported by previous studies.[17,50,51] Among the APU-BRDs, APU-ISA exhibited the highest ν_e (1831 mol/m^3), attributed to its difunctional monomer structure, which promoted a highly crosslinked network. In contrast, APU-VAA also showed a notably high ν_e (1550 mol/m^3), which can be ascribed to the presence of polar substituents on its aromatic ring, including —CHO, C=O, and —O— groups. These functional groups act as strong hydrogen bond acceptors, forming hydrogen bonds with the N—H groups in APU. Moreover, —CHO may react with urethane groups, further enhancing ν_e and restricting the segmental motion.[52] On the other hand, APU-PPA and APU-EGA displayed lower ν_e values of 752 mol·m^{-3} and 576 mol/m^3, respectively, both slightly below that of APU-IBOA (789 mol/m^3).

Gel content (GC) measurements (Table S4 in ESI) further support these trends. APU-ISA with difunctional monomer showed the highest GC (93.40%), while APU-VAA also exhibited a high GC (90.83%), likely due to the additional reactions involving the aldehyde group. In comparison, APU-PPA and APU-EGA presented relatively lower GC values of 86.34% and 83.57%, respectively. These results correlate well with the observed T_g, indicating that ν_e is the dominant factor influencing T_g variations. Although EGA contains an allyl group, its UV reactivity is considerably lower than that of methacrylate groups, resulting in partial participation in the crosslinking reaction during photopolymerization.

The TGA and DTG results (Fig. S13 and Table S6 in ESI) demonstrated that all APU-BRDs possessed good thermal stability, exhibiting two distinct decomposition stages in the ranges of 270–320 °C and 340–450 °C. Previous studies have reported that polyIBOA exhibits relatively poor thermal stability, with a maximum degradation peak around 300 °C.[53,54] However, when IBOA is copolymerized with bifunctional monomers to form a cross-linked network, the decomposition temperature is enhanced.[55] Typically, polyurethanes exhibit a maximum decomposition temperature around 400 °C.[56] Based on these findings, we infer that the first decomposition stage is primarily attributed to the radical degradation of the polymer, whereas the second stage corresponds to the depolymerization of the polyurethane segments. As illustrated in Fig. S13 (in ESI), the decomposition peaks of APU-BRDs around 300 °C are markedly lower than those of APU-IBOA, whereas the peaks in the 340–450 °C range are higher, indicating that APU-BRDs have superior thermal resistance compared to APU-IBOA.

Application for Electronic Watch Packaging

DPRA of APU-BRDs

When materials are used in electronic products that come in contact with the skin, it is crucial to assess their potential allergenicity. The DPRA of APU-BRDs, cysteine (Cys), and lysine (Lys)

channels were adopted. In the Cys channel (Table S7 in ESI), the positive control exhibited a depletion of 76.18%±1.52% (SD <14.9%), validating assay performance. Control peptides A (0.5087 mmol/L) and C (0.4985 mmol/L) consistently fell within the target range (0.45–0.55 mmol/L), while the combined peak-area coefficient of variation (CV) for Controls B+C (1.49%) confirmed high precision (<15% threshold). test sample reactivity was minimal, with a depletion of 1.49%±0.43% (SD <14.9%). Similarly, in the Lys channel (Table S8 in ESI), the positive control demonstrated 45.73%±1.41% depletion (SD <11.6%), and control peptides A (0.5062 mmol/L) and C (0.4998 mmol/L) met concentration specifications (0.45–0.55 mmol/L). The combined B+C peak-area CV (1.42%) and sample depletion (1.23%±1.18%, SD <11.6%) further supported assay reproducibility and negligible reactivity. Together, these results confirm robust experimental conditions and reliable test outcomes, with the observed reactivity classified as none to minimal.[57]

Lap shear test of APU-BRDs

Because smartwatch enclosures typically consist of a polycarbonate (PC) body and a glass cover, the adhesion behavior of APU-BRDs on PC-PC, glass-glass, and PC-glass was evaluated (Fig. 5a). Lap shear tests on these three types of materials revealed that, overall, APU-ISA and APU-VAA exhibited stronger bonding than APU-IBOA, whereas APU-PPA performed similarly to APU-IBOA. In contrast, APU-EGA showed a relatively lower adhesion strength. For all APU-BRDs, the highest lap shear strength was achieved when both the upper and lower substrates were PC, with cohesive failure occurring within the adhesive. When both substrates were glass, the shear strength was intermediate, and the lowest strength was observed in the PC-glass configuration, where interfacial failure consistently occurred on the glass side.

Taking APU-PPA as a representative example, the PC-PC joint exhibited a maximum shear strength of (19.02±0.59) MPa. This can be attributed to the formation of a robust interfacial layer through slight swelling and molecular interdiffusion between APU-BRDs and PC.[58] Furthermore, the relatively higher ductility of PC compared to glass enables elastic-plastic deformation during shear loading, which mitigates stress concentration. In contrast, the PC-glass configuration exhibited the lowest shear strength (8.47±0.15 MPa), likely owing to the significant mismatch in the elastic modulus and rigidity between the two substrates. This dissimilarity leads to an uneven stress distribution in the single-lap joint under a load. The high stiffness of the glass combined with the compliance of the PC induces bending and generates peel stress within the adhesive layer. As documented in the literature, such a stiffness mismatch in asymmetric joints exacerbates the interfacial stress concentration and reduces joint strength.[59]

To further explore the potential applications of APU-BRDs, their shear performance was assessed when both the upper and lower substrates were PMMA, PET, PE, aluminum, and ceramic (Fig. S14 in ESI). The results indicate that the APU-BRDs exhibit favorable adhesion to both PMMA and PET, with shear strengths intermediate between those observed on PC and glass. In contrast, the adhesion of APU-BRDs to low-surface-energy PE is considerably weaker. Aluminum foils and ceramics are commonly used substrates in electronic devices. Given that neither aluminum foil nor ceramic is transparent, UV curing is unsuitable for bonding homogeneous assemblies. Therefore, we separately measured the shear strengths of heterogeneous assemblies with PC. Clearly, the shear strength was close to that between PC and glass, and in all cases, failure occurred at the interface with the aluminum foil or ceramic side (Fig. S14 in ESI).

Wearable devices are frequently exposed to moisture, sweat, and personal care products during use, making the retention of strong adhesion critically important under such conditions. To evaluate this, lap-shear specimens bonded with APU-BRDs and APU-IBOA were immersed in a saline solution (0.9% NaCl) and glycerol for 7 days, after which their shear strengths were measured (Fig. 5b). Following immersion, APU-PPA, APU-VAA, and APU-ISA exhibited a decline in shear strength on PC-glass assemblies; however, all maintained values above 5.0 MPa, which is sufficient to ensure reliable adhesion under realistic wearable operating conditions. These formulations were similar to those used for APU-IBOA. In contrast, APU-EGA, which initially demonstrated the weakest bonding (only 7.22±1.58 MPa on PC-glass), suffered the most substantial reduction in adhesion after exposure, retaining only 72% of its original strength in glycerol and 54% in

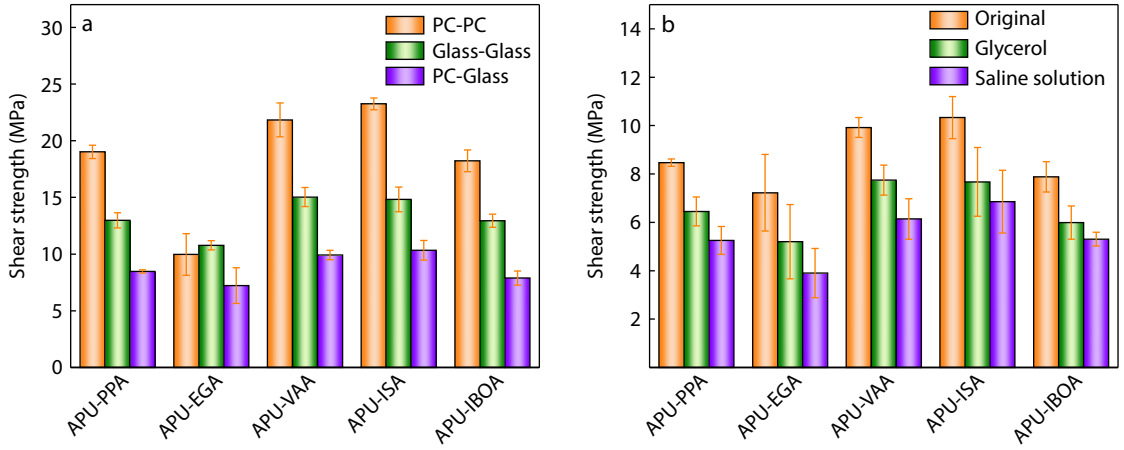

Fig. 5 (a) Shear strength of APU-BRDs and APU-IBOA on different substrates and (b) that of APU-BRDs and APU-IBOA on PC-glass configuration treated with glycerol and saline solution for 7 days.

saline. This pronounced loss can be attributed to its inherently poor interfacial interaction with the substrate and the lowest v_e and GC values (Table S4 in ESI). In the presence of polar media, such as water or glycerol, solvent molecules penetrate the adhesive-glass interface and preferentially interact with polar groups on the glass surface, displacing the hydrogen bonds originally formed between the adhesive and the substrate.

CONCLUSIONS

In this study, four novel bio-based reactive diluents (BRDs) derived from renewable feedstock (piperitol, vanillin, eugenol, and isosorbide) were synthesized. Structural characterization confirmed the successful preparation of these BRDs, which exhibited viscosities ranging from 5.1 mPa·s to 35.1 mPa·s and T_g of their corresponding polymers between 104 °C and 183 °C, effectively covering and surpassing the property ranges of conventional diluents such as IBOA and DMAA. An acrylate-terminated polyurethane (APU) matrix was synthesized using HMDI, PDGA, and HEA, and its structure was characterized. The incorporation of 22.5 wt% BRDs into the APU system resulted in a significant viscosity reduction from 3.57×10^5 mPa·s to a range of 5.2×10^4–9.85×10^4 mPa·s, corresponding to a viscosity drop of 72.4%–85.3%, performance comparable to that of IBOA. Mechanical testing of the cured APU-BRDs systems revealed tunable tensile strength and elongation at break, spanning 20.1–33.4 MPa and 82%–470%, respectively. More importantly, the adhesives demonstrated a superior bonding performance on various substrates. The shear strength on polar substrates such as PC reached up to 19.02 MPa. In a simulated smartwatch assembly (PC-glass bonding), the shear strength exceeded 8.47 MPa, with enhanced resistance to saline and glycerol exposure compared with IBOA-based reference systems. Critically, DPRA confirmed the non-irritating nature of the developed APU-BRDs. These comprehensive results underscore the potential of BRDs as effective and safer alternatives to petroleum-based diluents such as IBOA in this study system and are particularly suitable for skin-contact electronic device bonding applications.

Conflict of Interests

The authors declare no interest conflict.

Electronic Supplementary Information

Electronic supplementary information (ESI) is available free of charge in the online version of this article at http://doi.org/10.1007/s10118-026-3723-5.

Data Availability Statement

The data supporting the findings of this study are available from the corresponding author upon reasonable request.

ACKNOWLEDGMENTS

This study was financially supported by the Shandong Provincial Natural Science Foundation, China (Nos. ZR2022MB051 and ZR2021MB112), Postdoctoral Science Foundation of China (No. 2022M712343), Jinan City University Integration Development Strategy Project (No. JNSX2024030), Key Laboratory of Special Functional Aggregates of the Ministry of Education, Shandong University (No. JJT-2023-02), and Shandong SD-Link New Material Technology Co., Ltd.

REFERENCES

1 Moghaddam, F.; Tutunchi, A. The effect of modified silica nanoparticles on the mechanical properties of UV-curable polyurethane acrylate adhesive. *Int. J. Adhes. Adhes.* **2025**, *137*, 103899.
2 Zheng, K.; Wang, J.; Chen, J.; Hao, J.; Liu, Z.; Xing, S.; Yang, J.; Chen, D. High-strength and debondable UV-curable adhesive based on dual-dynamic network. *Polym. Degrad. Stabil.* **2025**, *242*, 111665.
3 Wang, G.; Zhou, Z.; Chen, M.; Wang, J.; Yu, Y. UV-curable polyurethane acrylate pressure-sensitive adhesives with high optical clarity for full lamination of TFT-LCD. *ACS Appl. Polym. Mater.* **2023**, *5*, 2051−2061.
4 Liu, Z.; Ju, C.; Li, P.; Yan, Z. C.; Zhang, Z. Disulfide-functionalized polyurethanes serve as UV-curable one-component adhesives. *J. Appl. Polym. Sci.* **2025**, *142*, e56520.
5 Choi, W. C.; Gavande, V.; Kim, D. Y.; Lee, W. K. Study on press formability and properties of UV-curable polyurethane acrylate coatings with different reactive diluents. *Polymers* **2023**, *15*, 880.
6 Baek, P.; Adler, B. L. Allergic contact dermatitis to isobornyl acrylate in a home nail glue. *Contact Dermatitis* **2024**, *91*, 64−66.
7 Kamann, S.; Oppel, E.; Liu, F.; Reichl, F. X.; Heinemann, L.; Högg, C. Evaluation of isobornyl acrylate content in medical devices for diabetes treatment. *Diabetes Technol. Ther.* **2019**, *21*, 533−537.
8 Yadav, S. K.; Schmalbach, K. M.; Kinaci, E.; Stanzione, J. F.; Palmese, G. R. Recent advances in plant-based vinyl ester resins and reactive diluents. *Eur. Polym. J.* **2018**, *98*, 199−215.
9 Pérocheau Arnaud, S.; Malitowski, N. M.; Meza Casamayor, K.; Robert, T. Itaconic acid-based reactive diluents for renewable and acrylate-free UV-curing additive manufacturing materials. *ACS Sustainable Chem. Eng.* **2021**, *9*, 17142−17151.
10 He, Q.; Hu, L.; Huang, Y.; Huang, T.; Zhu, Z.; Li, Y.; Hu, Y.; Yang, Z. Eugenol-based multi-functional monomer as reactive diluent for high bio-content UV-curable coatings. *Prog. Org. Coat.* **2025**, *200*, 109079.
11 Yu, A. Z.; Serum, E. M.; Renner, A. C.; Sahouani, J. M.; Sibi, M. P.; Webster, D. C. Renewable reactive diluents as practical styrene replacements in biobased vinyl ester thermosets. *ACS Sustainable Chem. Eng.* **2018**, *6*, 12586−12592.
12 Wu, J.; Qian, Y.; Sutton, C. A.; La Scala, J. J.; Webster, D. C.; Sibi, M. P. Bio-based furanic di(meth)acrylates as reactive diluents for UV curable coatings: Synthesis and coating evaluation. *ACS Sustainable Chem. Eng.* **2021**, *9*, 15537−15544.
13 Dai, Z.; Li, Q.; Chen, Z.; Shawon, R. K.; Zhu, Y.; Lv, H.; Fu, F.; Zhu, Y.; Fu, Y.; Liu, X. Reactive diluent derived from ferulic acid for the preparation of a fully biobased unsaturated polyester resin. *ACS Sustainable Chem. Eng.* **2020**, *8*, 17379−17386.
14 Zhang, C.; Zhang, Y.; Liu, Y.; Cui, Y.; Zhao, M.; Peng, S.; Wang, H.; Song, Z.; Zhang, Q.; Shi, D.; Zhu, Y. Effects of polyol types on underwater curing properties of polyurethane. *Polymers* **2025**, *17*, 5.
15 Li, S.; Liu, Z.; Hou, L.; Chen, Y.; Xu, T. Effect of polyether/polyester polyol ratio on properties of waterborne two-component polyurethane coatings. *Prog. Org. Coat.* **2020**, *141*, 105545.
16 Li, G.; Duan, B.; Leng, G.; Liu, J.; Zhang, T.; Lu, Z.; Wang, S.; Qu, J.

Graphical Abstract

Investigation of Bio-based Acrylate Reactive Diluents for UV-curable Electronic Packaging Polyurethane Adhesives

Yun-Tao Li, Shun-Peng Sun, Ya-Meng Jia, Shu-Sheng Li, Chuan-Yong Zong, Xu-Bao Jiang, and Xiao-Li Zhu

University of Jinan; Shandong University; Shandong Link Adhesive Co., Ltd.

By replacing traditional diluents with bio-based reactive diluents and compounding them with acrylate-terminated polyurethane, a UV-curable adhesive suitable for smart wearable devices is obtained.

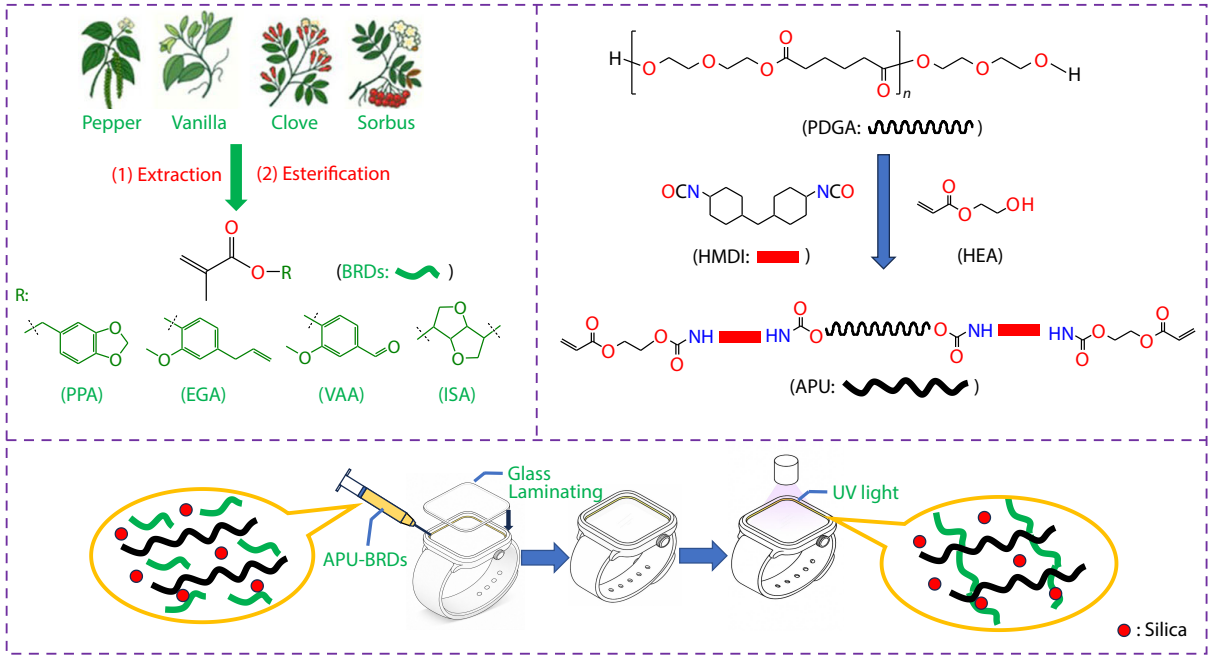

Chinese J. Polym. Sci., 2026 *https://doi.org/10.1007/s10118-026-3723-5*

Preparation of yellowing-resistant waterborne polyurethane modified with disulfide bonds. *Molecules* **2024**, *29*, 2099.

17 Wang, H.; Cao, L.; Wang, X.; Lang, X.; Cong, W.; Han, L.; Zhang, H.; Zhou, H.; Sun, J.; Zong, C. Effects of isocyanate structure on the properties of polyurethane: Synthesis, performance, and self-healing characteristics. *Polymers* **2024**, *16*, 3045.

18 Droesbeke, M. A.; Aksakal, R.; Simula, A.; Asua, J. M.; Du Prez, F. E. Biobased acrylic pressure-sensitive adhesives. *Prog. Polym. Sci.* **2021**, *117*, 101396.

19 Stanzione, J. F.; Sadler, J. M.; La Scala, J. J.; Wool, R. P. Lignin model compounds as bio-based reactive diluents for liquid molding resins. *ChemSusChem* **2012**, *5*, 1291–1297.

20 Gomez-Lopez, A.; Grignard, B.; Calvo, I.; Detrembleur, C.; Sardon, H. Synergetic effect of dopamine and alkoxysilanes in sustainable non-isocyanate polyurethane adhesives. *Macromol. Rapid Comm.* **2021**, *42*, 2000538.

21 Wang, T.; Deng, H.; Li, N.; Xie, F.; Shi, H.; Wu, M.; Zhang, C. Mechanically strong non-isocyanate polyurethane thermosets from cyclic carbonate linseed oil. *Green Chem.* **2022**, *24*, 8355–8366.

22 Mousa, A.; Karger-Kocsis, J. Cure characteristics of a vinyl ester resin as assessed by FTIR and DSC techniques. *Polym. Polym. Compos.* **2000**, *8*, 455–460.

23 Stanzione Iii, J. F.; Sadler, J. M.; La Scala, J. J.; Reno, K. H.; Wool, R. P. Vanillin-based resin for use in composite applications. *Green Chem.* **2012**, *14*, 2346–2352.

24 Marcelis, Q.; Deconinck, E.; Rogiers, V.; Vanhaecke, T.; Desmedt, B. Applicability of the DPRA on mixture testing: Challenges and opportunities. *Arch. Toxicol.* **2023**, *97*, 2453–2461.

25 Sakakura, A.; Kawajiri, K.; Ohkubo, T.; Kosugi, Y.; Ishihara, K. Widely useful DMAP-catalyzed esterification under auxiliary base- and solvent-free conditions. *J. Am. Chem. Soc.* **2007**, *129*, 14775–14779.

26 Sivabalan, P.; Kozody, M. J.; Yuya, P.; Samways, D. S. K.; Shipp, D. A. Synthesis of soluble poly(methacrylic anhydride) by radical cyclopolymerization. *Macromolecules* **2024**, *57*, 3985–3992.

27 Xu, C. A.; Liang, W.; Wu, X.; Jiao, E.; Lu, M.; Wu, K.; Hao, X.; Shi, J. Effect of novel silicone/vanillin monomer on the thermal stability and adhesion properties of UV-curable polyurethane pressure sensitive adhesive and its application in functional glass. *Prog. Org. Coat.* **2022**, *171*, 107019.

28 Jašek, V.; Fučík, J.; Krhut, J.; Mravcova, L.; Figalla, S.; Přikryl, R. A

study of isosorbide synthesis from sorbitol for material applications using isosorbide dimethacrylate for enhancement of bio-based resins. *Polymers* **2023**, *15*, 3640.
29 Sadler, J. M.; Nguyen, A. P. T.; Toulan, F. R.; Szabo, J. P.; Palmese, G. R.; Scheck, C.; Lutgen, S.; La Scala, J. J. Isosorbide-methacrylate as a bio-based low viscosity resin for high performance thermosetting applications. *J. Mater. Chem. A* **2013**, *1*, 12579–12586.
30 Alvarez, F.; Colmenero, J.; Wang, C. H.; Xia, J. L.; Fytas, G. Segmental dynamics in bulk poly(isobomyl methacrylate) and its random copolymer with poly(methyl methacrylate) near T_g. *Macromolecules* **1995**, *28*, 6488–6493.
31 Yang, T. P.; Pearce, E. M.; Kwei, T. K.; Yang, N. L. Complexation of poly(*N,N*-dimethylacrylamide) and phenol-formaldehyde resins. *Macromolecules* **1989**, *22*, 1813–1818.
32 Badía, A.; Santos, J. I.; Agirre, A.; Barandiaran, M. J.; Leiza, J. R. UV-tunable biobased pressure-sensitive adhesives containing piperonyl methacrylate. *ACS Sustainable Chem. Eng.* **2019**, *7*, 19122–19130.
33 Rodrigo, A. B. Development of waterborne polymeric dispersions based on biobased monomers for their application as PSAs and coatings. University of the Basque Country UPV/EHU, Donostia-San Sebastián, **2020**.
34 Petersen, S. R.; Prydderch, H.; Worch, J. C.; Stubbs, C. J.; Wang, Z.; Yu, J.; Arno, M. C.; Dobrynin, A. V.; Becker, M. L.; Dove, A. P. Ultra-tough elastomers from stereochemistry-directed hydrogen bonding in isosorbide-based polymers. *Angew. Chem. Int. Ed.* **2022**, *61*, e202115904.
35 Jašek, V.; Bartoš, O.; Prokeš, J.; Kameníková, E.; Přikryl, R.; Figalla, S. Sustainable and highly efficient synthesis of reactive diluents from renewable sources for property-enhancing purposes in glass-containing material composites. *Precis. Chem.* **2026**, *4*, 1–12.
36 Jašek, V.; Lavrinčíková, V.; Prokeš, J.; Bartoš, O.; Přikryl, R.; Figalla, S. Green photocurable vegetable oil biobased thermoset functionalized with vanillin methacrylate for ultraviolet-shielding coatings. *ACS Appl. Polym. Mater.* **2025**, *7*, 11925–11937.
37 Molina-Gutiérrez, S.; Dalle Vacche, S.; Vitale, A.; Ladmiral, V.; Caillol, S.; Bongiovanni, R.; Lacroix- Desmazes, P. Photoinduced polymerization of eugenol- derived methacrylates. *Molecules* **2020**, *25*, 3444.
38 Rigo, E.; Ladmiral, V.; Caillol, S.; Lacroix-Desmazes, P. Recent advances in radical polymerization of bio-based monomers in aqueous dispersed media. *RSC Sustainability* **2023**, *1*, 788–813.
39 Zhu, A.; Shi, L.; Shi, H.; Qian, J.; Shi, Y. Role of the soft and hard segments structure in modifying the performance of acrylic adhesives modified by polyurethane macromonomers. *ACS Omega* **2024**, *9*, 32735–32744.
40 Feng, S.; Yang, H.; Qiu, Z. Novel biobased poly(hexamethylene-*co*-diethylene glycol furandi- carboxylate) copolyesters with improved mechanical properties and hydrolytic degradation rates. *Polym. Chem.* **2025**, *16*, 2133–2142.
41 Lu, M.; Zhu, X.; Li, X.; Yang, X.; Tu, Y. Synthesis of cyclic oligo(ethylene adipate)s and their melt polymerization to poly(ethylene adipate). *Chinese J. Polym. Sci.* **2017**, *35*, 1051–1060.
42 Jing, P.; Du, J.; Miao, D.; Xiao, G.; Jiang, Y.; Xu, C. Polyurethanes based on dicyclohexylmethane 4,4′-diisocyanate and *N*-*tert*-butyldiethanolamine for enhancing the dyeability of fiber toward acid dye. *ACS Appl. Polym. Mater.* **2023**, *5*, 1276–1282.
43 Yin, F. M.; Wu, L. L.; Li, S. S.; Pan, X. N.; Zhu, X. L.; Jiang, X. B.; Kong, X. Z. Unconventional fluorescent and multi-responsive polyethyleneimine with LCST and UCST behavior: Synthesis, characterization and biological applications. *Chinese J. Polym. Sci.* **2024**, *42*, 826–837.
44 Li, X. D.; Li, S. S.; Jiang, X. B.; Zhu, X. L.; Kong, X. Z. Unconventional fluorescent and multi-responsive polysiloxane: Synthesis, characterization and biological applications. *Chinese J. Polym. Sci.* **2024**, *42*, 579–590.
45 Li, L.; Li, S.; Cui, H.; Zhu, X.; Kong, X. Z. Phase transition and fluorescence emission of multiresponsive poly(ethylene glycol-*co*-siloxane) and its application for uric acid detection. *ACS Appl. Polym. Mater.* **2023**, *5*, 9413–9424.
46 Wu, Y.; Fan, L.; Chen, Y.; Zhang, X.; Chen, D.; Yang, W. Branching structured poly(vinyl chloride-*co*- hydroxyethyl acrylate)-*g*-polycaprolactone as nonmigratory polymeric plasticizers and compatibilizers in flexible PVC. *ACS Appl. Polym. Mater.* **2025**, *7*, 1039–1051.
47 Zvonkina, I. J.; Hilt, M. Tuning the mechanical performance and adhesion of polyurethane UV cured coatings by composition of acrylic reactive diluents. *Prog. Org. Coat.* **2015**, *89*, 288–296.
48 Tian, M.; Gao, Y.; Liu, Y.; Liao, Y.; Hedin, N. E.; Fong, H. Fabrication and evaluation of Bis-GMA/TEGDMA dental resins/composites containing nano fibrillar silicate. *Dent. Mater.* **2008**, *24*, 235–243.
49 Topa-Skwarczyńska, M.; Ortyl, J. Photopolymerization shrinkage: Strategies for reduction, measurement methods and future insights. *Polym. Chem.* **2023**, *14*, 2145–2158.
50 Saville, B.; Watson, A. A. Structural characterization of sulfur-vulcanized rubber networks. *Rubber Chem. Technol.* **1967**, *40*, 100–148.
51 Kannurpatti, A. R.; Anderson, K. J.; Anseth, J. W.; Bowman, C. N. Use of ''living'' radical polymerizations to study the structural evolution and properties of highly crosslinked polymer networks. *J. Polym. Sci. B* **1997**, *35*, 2297–2307.
52 Banan, A. R.; Keshavarz, S. M. Biobased self healing waterborne polyurethane with vanillin derived dynamic imine bonds for enhanced mechanical strength and performance. *Sci. Rep.* **2025**, *15*, 33255.
53 Merah, D.; Bedjaoui, L.; Zeggai, N.; Bouberka, Z.; Sarazin, J.; Boutalbi, D.; Barrera, A.; Boughrara, H.; Dubois, F.; Cazaux, F.; Supiot, P.; Maschke, U. Enhanced thermal stability of biobased crosslinked poly (isobornylacrylate-*co*-2-ethylhexylacrylate) copolymers. *J. Polym. Res.* **2022**, *29*, 279.
54 Ors, J. A.; Perriere, D. M. L. Thermogravimetric profile of decomposition of acrylate systems based on bornyl acrylate monomers. *Polymer* **1986**, *27*, 1999–2002.
55 Zeggai, N.; Dali Youcef, B.; Dubois, F.; Bouchaour, T.; Supiot, P.; Bedjaoui, L.; Maschke, U. Analysis of dynamic mechanical properties of photochemically crosslinked poly(isobornylacrylate-*co*-isobutylacrylate) applying WLF and Havriliak-Negami models. *Polym. Test.* **2018**, *72*, 432–438.
56 Herrera, M.; Matuschek, G.; Kettrup, A. Thermal degradation of thermoplastic polyurethane elastomers (TPU) based on MDI. *Polym. Degrad. Stabil.* **2002**, *78*, 323–331.
57 Xie, C.; Li, L. Y.; Li, S. S.; Zong, C. Y.; Jiang, X. B.; Zhu, X. L.; Feng, S. Y.; Kong, X. Z. Poly(hydroxy urethane-siloxane) pressure-sensitive adhesive: Synthesis, characterization and its usage for skin-contact sensors. *Chinese J. Polym. Sci.* **2026**, *44*, 536–548.
58 Léger, L.; Creton, C. Adhesion mechanisms at soft polymer interfaces. *Phil. Trans. R. Soc. A* **2008**, *366*, 1425–1442.
59 Ma, G.; Wu, J.; Yuan, H. Interfacial shear stress analysis in single-lap adhesive joints with similar and dissimilar adherends under dynamic loading. *Int. J. Adhes. Adhes.* **2021**, *111*, 102953.